Purity Assessment of Single-Wall Carbon Nanotubes, Using Optical Absorption Spectroscopy

Brian J. Landi,[†,‡] Herbert J. Ruf,[†] Chris M. Evans,[†] Cory D. Cress,[†,‡] and Ryne P. Raffaelle*[,†,‡]

NanoPower Research Laboratories (NPRL), Rochester Institute of Technology, Rochester, New York 14623, and Microsystems Engineering, Rochester Institute of Technology, Rochester, New York 14623

Received: November 2, 2004; In Final Form: March 25, 2005

A demand currently exists for a method of assessing the purity of single-wall carbon nanotubes (SWNTs), which will allow for meaningful material comparisons. An established metric and protocol will enable accurate and reproducible purity claims to be substantiated. In the present work, the ability to accurately quantify the mass fraction of SWNTs in the carbonaceous portion of a given sample is demonstrated, using optical absorption spectroscopy on both laser and arc discharge-generated SWNT-*N*,*N*-dimethylacetamide (DMA) dispersions. Verification of purity assessment protocols is based upon constructed sample sets comprising designed mass fractions of purified SWNTs and representative carbonaceous synthesis byproducts. Application of a previously reported method (Itkis et al. *Nano Lett.* **2003**, *3*, 309) based on a ratio of the areal absorbance from linear subtractions of the second interband electronic transitions of semiconducting SWNTs ($^{S}E_{22}$) has shown a severe overestimation of SWNT purity (average error >24%). Instead, the development of a nonlinear π-plasmon model, which considers overlap of electronic transitions and peak broadening, has dramatically improved the purity assessment accuracy (average error <7%), derived from a strong correlation to the constructed sample sets. This approach has enabled corroboration of rapid assessment procedures, such as absorbance peak maxima ratio and Beer's law analysis, directed at purification monitoring and synthesis sample screening. Specifically, a simple protocol for purity assessment of laser and arc-discharge SWNTs has been established that can be extended to other synthetic types (i.e. CVD, HiPco, etc.) and diameter distributions.

Introduction

The unique electrical, optical, and mechanical properties inherent to single-wall carbon nanotubes (SWNTs) have garnered tremendous interest in basic science and applied research.[1−3] Although a variety of experimental methods can be employed in the fabrication of SWNTs (i.e. arc-discharge, chemical vapor deposition, and pulsed laser vaporization), each technique produces SWNTs with differing diameter, chirality distributions, and various amounts of synthesis byproducts.[2] In general, the byproducts are the principal component of the as-produced materials or raw SWNT "soot". Byproducts such as graphitic and amorphous carbon phases, metal catalysts, fullerenes, and carbonaceous coatings on the SWNTs may not only dominate the physical characteristics of the raw soot, but they also pose significant challenges in any subsequent purification.[4−10] Further development of SWNT-based applications is expected to require material standardization, specifically with respect to electronic type and degree of purity. Consequently, there is a need to develop a method whereby the types, amount, and morphology of SWNT-containing materials can be accurately and precisely quantified.[11]

Several different qualitative and semiquantitative techniques have been used thus far to characterize the physical properties of SWNT-containing samples.[11−15] Techniques such as scanning electron microscopy (SEM), transmission electron microscopy (TEM), UV−vis−NIR spectroscopy, thermogravimetric analysis (TGA), and Raman spectroscopy have been routinely employed independently or in combination.[11] Additionally, various attempts have been made to extract information regarding the "purity" of a sample based on these measurements. However, disparate results and definitions of what constitutes purity have appeared in the literature, with some reports citing SWNT volume percent from microscopy measurements,[12,14] while others state relative weight percent derived from the decomposition residue of TGA.[6] The implication is that many groups have used such techniques to report high purity levels, with several accounts greater than 90% "pure" without reference to adequate standardization.[6,7,13,15−17] Therefore, it is essential that a precise definition be established for both measurement and terminology as to what "purity" means in regard to SWNTs. Ultimately, the definition of purity is application-specific where some may require single chirality (n, m) SWNTs, while others desire electronic type-pure (semiconducting or metallic). The most basic definition and the focus of this paper is to describe "purity" as the total mass fraction (w_{SWNTs}) of SWNTs contained in a sample.

Purity assessment of SWNTs should rely on techniques which analyze a representative portion of the SWNT-containing sample and measure quantities which are specific to the components of interest. In addition, a reference standard is necessary to validate the techniques and ensure assessment reproducibility. Although verification of the metal catalyst impurity levels has been shown with TGA and energy-dispersive X-ray analysis (EDX), a precise determination of the relative quantities of carbonaceous constituents has not been unambiguously

* Address correspondence to this author. E-mail: rprsps@rit.edu.
† NPRL.
‡ Microsystems Engineering.

10.1021/jp044990c CCC: $30.25
Published on Web 04/21/2005

demonstrated.[4−7,9,18] Microscopy approaches such as TEM and SEM are also insufficient due to the extremely limiting sample sizes (estimated to be 10^{-12} g SWNTs per image at 20000×).[19] Using Raman spectroscopy, it has been proposed that a relation between the tangential mode shift and laser power density can be used as a means to quantify the relative SWNT fraction in a carbon-containing sample.[14,20] Other work has suggested that a correlation exists between the ratio of the peak intensities for the D- and G-Bands and the purity of a SWNT-containing sample.[12,21−24] However, the effects of non-SWNT carbon on the resonance Raman data for a given sample can significantly affect the D:G ratio, as demonstrated for mixtures of SWNTs with multiwalled carbon nanotubes (MWNTs).[23] Additionally, it is well established that the resonant Raman process is a powerful technique for determining individual diameters and electronic types, but is also very specific to the incident laser energy.[25] Therefore, the applicability of Raman spectroscopy for the bulk analysis of a sample is not straightforward. Such an analysis would require the convolution of multiple measurements over the necessary range of excitation energies to resonantly enhance the entire diameter and electronic type distribution in a given sample. In contrast, optical absorption spectroscopy can probe the entire SWNT sample in a single measurement, indicating the presence of each diameter and electronic type.[26] These properties manifest as distinct spectral features unique to the electronic transitions corresponding to Van Hove singularities for each SWNT.[27]

The use of stable SWNT−organic solvent dispersions in optical absorption spectroscopy allows for a quantitative solution-phase analysis, provided that concentrations are below SWNT−solvent dispersion limits.[28] Selection of an appropriate organic solvent permits homogeneous sampling without chemical functionalization and simple sample recovery. A recent report on this approach to purity assessment has proposed that the degree of SWNTs present in a sample can be directly related to the absorbance of the interband electronic transitions corresponding to the semiconducting peak at the energy of the 2nd Van Hove singularity ($^{S}E_{22}$).[19] Although any of the prominent peaks are stated as being applicable, selection of the $^{S}E_{22}$ peak has been proposed in ref 19 based on the mitigation of chemical doping effects which can be observed for the $^{S}E_{11}$ peak. The purity assessment was performed by comparing raw electric arc discharge (EA) SWNT samples against a "high purity" reference sample in *N*,*N*-dimethylformamide (DMF) solvent dispersions at 10 μg/mL. Calculation of the reference sample's ratio of areal absorbance for the linearly subtracted region [AA($^{S}E_{22}$)] and total areal absorbance [AA(T)] of the $^{S}E_{22}$ peak over selected spectral cutoffs is proposed as the calibration standard. A comparison of the raw EA SWNTs' areal absorbance to the reference ratio is then used to assess purity, with a reported reliability of this method for raw EA SWNTs to be within 3%. Unfortunately, this approach uses a nonphysically based linear subtraction at the peak minima to approximate the relative electronic transitions of the SWNTs, and the underlying absorption from the π-plasmon.[19,29−33] (Also, the analysis only evaluates the $^{S}E_{22}$ peak, thereby excluding higher energy metallic SWNT transitions which may influence the results.) Other work using optical absorption spectroscopy has investigated the spectral features from ∼1−5 eV for aqueous surfactant suspensions and employed a nonphysically based parabolic curve fit as the background subtraction from an iterative selection of the minima between SWNT peaks for points at ∼450, 610, and 820 nm.[34] The calculation for SWNT abundance involves integration of the peak area under the $^{M}E_{11}$ peak after parabolic subtraction for a reference sample, enabling a relative comparison for other samples. This type of approach arbitrarily forces the minima to an artificial baseline, discounting the possibility for differences in overlap of electronic transitions between peaks.[34] However, the shortcomings of these specific approaches aside, there is the larger issue surrounding purity assessment in general, which is the lack of any calibration standard to verify the accuracy of a given approach.

In the current study, SWNTs produced by the pulsed laser vaporization process and commercially available arc-discharge (Carbon Solutions, Inc.) were analyzed by using solvent dispersions in *N*,*N*-dimethylacetamide (DMA). The results from UV−vis−NIR spectroscopy of SWNT−DMA dispersions, at concentrations below the dispersion limit, have shown highly resolved spectra, [28] which can enable the subsequent deconvolution of the peaks corresponding to both the semiconducting and metallic types. Identification of an appropriate nonlinear model for the π-plasmon absorption has allowed for a physically based background subtraction over the entire range of SWNT electronic transitions in the solvent transmission window. This nonlinear model has been applied to estimating the SWNT weight fraction of carbonaceous material ($^{c}w_{SWNTs}$) for constructed sample sets comprising designed mass fractions of purified laser-SWNTs and nanostructured carbon, as well as purified arc-SWNTs and carbon soot (Aldrich) to validate the methodology. In addition, the analysis of these sample sets with regard to experimental extinction coefficients, absorption intensity, and peak tie line slopes show promise as rapid assessment protocols. Application of both nonlinear and rapid purity assessment methods to raw laser and raw arc-SWNT soot was also investigated. An extension of this analysis can lead to SWNT electronic type ratio and quantitative information on individual diameter concentrations for a given SWNT sample. Overall, this approach is expected to establish an accurate comparison of experimental results, provide the ability for optimization of synthesis and purification,[29−31] and ultimately initiate the realization of standardized levels of purity.

Experimental Section

Synthesis and Purification. Single-wall carbon nanotubes were synthesized using the pulsed laser vaporization technique (L-SWNTs), employing an Alexandrite laser (755 nm). The laser pulse was rastered (corner to corner over 1 cm^2 with 50% overlap of 100 μs pulses at a repetition rate of 10 Hz) over the surface of a graphite (1−2 μm) target doped with 2% w/w Ni (submicron) and 2% w/w Co (<2 μm), at an average power density of 100 W/cm^2. The reaction furnace temperature was maintained at 1150 °C, with a chamber pressure of 700 Torr under 100 cm^2 flowing Ar in a 46 mm inner diameter (50 mm outer diameter) quartz tube.[28] Synthesis of a representative nanostructured carbon (NC) component in the raw L-SWNT soot was performed by laser vaporization at the described conditions for an undoped graphite target. For comparison of material properties and purity assessment protocols from commercial sources, a batch of arc-discharge SWNTs (A-SWNTs) was purchased from Carbon Solutions, Incorporated.[35] The corresponding non-SWNT carbon representative of the arc-discharge process was used in the form of carbon soot (CS), made from the resistive heating of graphite rods, and purchased from Aldrich.

Purification of both L- and A-SWNT raw soots was performed based on a previously reported procedure.[28] In summary, 50−100 mg of each raw SWNT soot was brought to reflux at 120 °C in 3M nitric acid for 16 h, and then filtered over a 1

μm PTFE membrane filter with copious amounts of water. The membrane filters were dried at 70 °C in vacuo to release the resulting SWNT papers from the filter paper. The L-SWNT paper was thermally oxidized in air at 450 °C for 1 h in a Thermolyne 1300 furnace, followed by a 6 M hydrochloric acid wash for 30 min, using magnetic stirring, equivalent filtering steps, and a final oxidation step at 550 °C for 1 h. In the case of the A-SWNTs, a sequential series of thermal oxidations at 450, 525, and 600 °C occurred for 1 h each, with intervening 6 M HCl acid wash and filtering steps being performed. The typical purification yield for the laser raw soot was 10% w/w and the arc raw soot was 2% w/w; however, concern for the quality of purified material was a larger consideration than optimization of this purification process.

Material Characterization. Characterization of the SWNTs, NC, and CS was performed by scanning electron microscopy (SEM), Raman spectroscopy, and thermogravimetric analysis (TGA). The SEM was performed at 2 kV using a Hitachi S-900, with samples applied directly to the brass stub with use of silver paint. Raman spectroscopy was performed at room temperature, using a JY-Horiba Labram spectrophotometer from 100 to 2800 cm^{-1} with excitation energies of 1.96 (He/Ne) and 2.54 eV (Ar). These energies have been shown to probe both the metallic and semiconducting SWNTs, respectively, over the range of diameters for L- and A-SWNTs used in this study.[25] Thermogravimetric analysis (TGA) was conducted with a TA Instruments 2950. Samples were placed in the platinum pan balance in quantities of ~1 mg and ramped at 10 °C/min from room temperature up to 950 °C under air at a gas flow rate of 60 sccm.

Optical Absorption and Constructed Sample Sets. UV−vis−NIR spectra were obtained on stable dispersions of SWNTs, NC, and CS in *N*,*N*-dimethylacetamide (DMA) and an air sprayed sample on a quartz slide from a 0.1 mg/mL SWNT−acetone solution, using a Perkin-Elmer Lambda 900 spectrophotometer.[28] Sample handling for dispersion solutions involved the use of 1 cm quartz cuvettes. Data were obtained over an energy range of 0.90−4.25 eV, corresponding to the transmission window of the alkyl amide solvent. Given the fact that the spectrophotometer is only measuring optical transmittance during these measurements, the possibility exists that scattering in the dispersions will affect the absorption data. Although the effects of particle scattering are quite pronounced on sprayed SWNT samples (>30%),[36] previous reports indicate that scattering on SWNT dispersions is negligible at concentrations of 10 μg/mL in DMF[19] and 20 μg/mL in aqueous surfactant dispersions.[36] Therefore, the dispersion concentration employed presently of 2.5 μg/mL should exhibit even less spectral distortion due to scattering than those reported. The constructed laser sample set was prepared from a volumetric mixture of a 2.5 μg/mL stock solution of purified L-SWNTs in DMA with a 2.5 μg/mL stock solution of NC-DMA in 20% increments (i.e. concentrations of 0%, 20%, 40%, 60%, 80%, and 100% w/w SWNTs). The same procedure was also employed for preparation of the constructed arc sample set with volumetric mixing of a 2.5 μg/mL purified A-SWNT-DMA dispersion with a 2.5 μg/mL stock solution of CS-DMA. The raw L- and A-SWNT soots were also analyzed from 2.5 μg/mL DMA dispersions. Each of these concentrations reflects the mass of carbon containing material calculated from the TGA data, adjusting for the relative mass of metal oxides (assuming Ni/Co metal in laser raw soot is 72% and Ni/Y metal in arc raw soot is 75% of the residual oxide value for 50:50 metal catalyst mixtures) as determined by the decomposition residue.

Fullerene Extraction. Evaluation of the C_{60} fullerene content in the carbonaceous samples was performed by a toluene extraction and analysis by optical absorption spectroscopy based on the reported extinction coefficient ($\epsilon = 54\,200\ M^{-1}\ cm^{-1}$ at 336 nm for C_{60} in toluene).[37] The carbonaceous samples were prepared at concentrations of ~0.25 mg/mL in toluene (an order of magnitude below the solubility limit of C_{60} in toluene of 2.8 mg/mL[38]) and placed in an ultrasonic bath for 20 min at 25 °C. After centrifugation for 10 min at 5000 rpm, the supernatant was analyzed to determine the soluble fullerene content in toluene.

Results and Discussion

The accuracy of purity assessment methods can be validated by appropriate characterization with a reference SWNT sample set. As stated previously, the opportunity to acquire a 100% w/w pure SWNT sample is currently not available,[19] thereby necessitating an alternative reference. In the present case, a reference sample set has been constructed where various SWNT mass fractions are achieved through the mixtures of purified SWNTs and representative carbonaceous byproducts. Purified laser (L-) and arc (A-) SWNTs were prepared by standard purification treatment and shown to possess a high degree of purity and material quality based on conventional microscopy and spectroscopy. The absolute degree of purity of the purified SWNTs is obviously unknown. However, verification of the assessment method is not dependent on the absolute quality of the purified SWNTs, but is based on the correlation of purity estimates with designed fractions in the constructed sample sets. The purity assessment protocols will remain valid even with other reference samples of potentially higher purity.[19]

Material Characterization and Constructed Sample Sets. Initially, microscopic and spectroscopic characterization was performed on the raw SWNTs, purified SWNTs, and representative carbonaceous synthesis impurities (i.e., nanostructured carbon (NC) for laser synthesis and carbon soot (CS) for arc-discharge synthesis) to identify corresponding sample morphologies and physical properties. Shown in Figure 1 are the SEM images of (a) raw L-SWNTs, (b) raw A-SWNTs, (c) purified L-SWNTs, (d) purified A-SWNTs, (e) NC, and (f) CS. Evident from the raw L-SWNTs are the highly entangled bundles of SWNTs with the obvious presence of amorphous carbon and metal catalyst impurities. Similar morphologies are seen with the raw A-SWNTs, although the observed quantity of SWNTs is generally lower than in the case of L-SWNTs. The purified SWNTs in both cases show highly ordered, well-defined bundles with trace metal particles present. Analysis of the SEM images for NC and CS shows nearly identical surface morphology with globular particles and the absence of any carbon nanotube materials. The TGA data (see Figure S1 in the Supporting Information) show significantly higher metal catalyst impurities in the raw A-SWNTs compared to the raw L-SWNTs (31.9% w/w vs 10.2% w/w, respectively). The purified A- and L-SWNTs show residual impurities of 16.9% w/w and 11.7% w/w, respectively, and significantly higher carbonaceous decomposition temperatures compared to the raw soots based on the 1st derivative plots (i.e., 730 and 767 °C, respectively). The NC and CS TGA data show nearly complete carbonaceous decomposition by ~625 °C; however, the presence of graphitic material is apparent in the CS with a minor decomposition transition at ~700 °C.

Raman spectroscopy was performed on each of the material types using a He/Ne 1.96 eV laser and the spectra are shown in Figure 2. The pronounced D- (~1300 cm^{-1}) and G-Bands

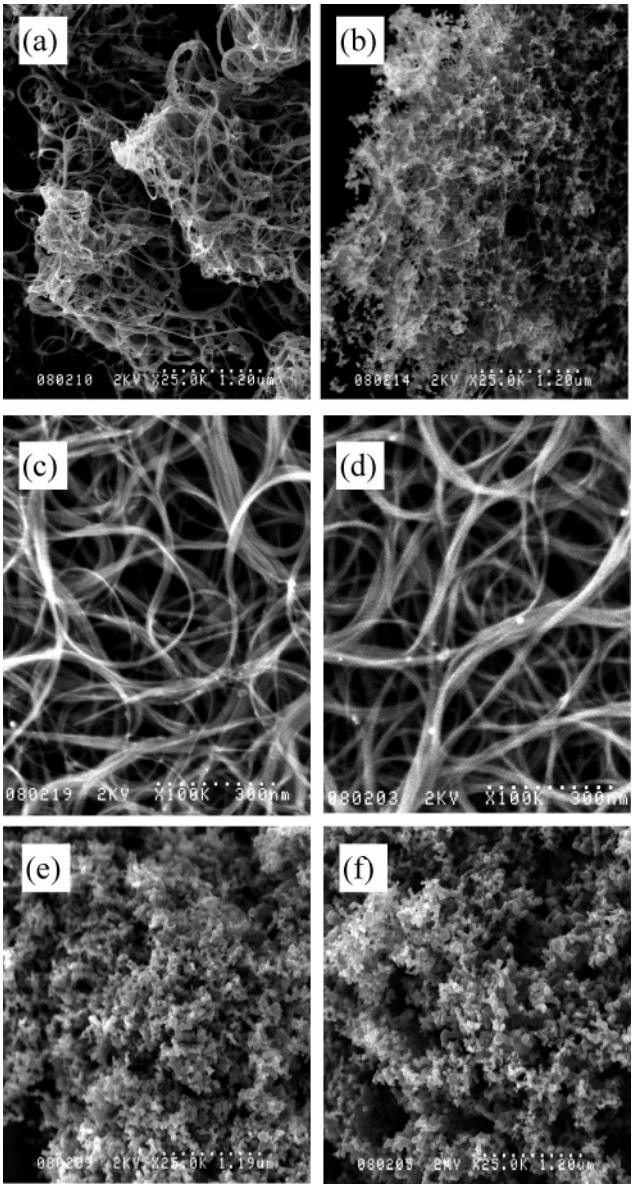

Figure 1. SEM images for (a) raw L-SWNT soot, (b) raw A-SWNT soot (Carbon Solutions, Inc.), (c) purified L-SWNTs, (d) purified A-SWNTs, (e) nanostructured carbon (NC), and (f) carbon soot (CS-Aldrich). The magnifications for a, b, e, and f are 25000× while c and d are 100000×.

(∼1600 cm^{-1}) are evident in the NC and CS samples with a higher relative intensity around 500 cm^{-1} for the CS attributed to increased fullerene content.[38] This observation was confirmed by the toluene extraction of soluble C_{60} fullerenes where NC and CS contain 2.6% w/w and 3.6% w/w, respectively. The absence of a radial breathing mode (RBM) (∼120−200 cm^{-1}) for both NC and CS samples supports the notion that these samples lack any SWNTs. In comparison, the typical spectra for SWNTs is observed in both purified arc and laser with the prominent RBM peaks, G- (∼1400−1600 cm^{-1}) and G′-Bands (∼2600 cm^{-1}), being distinctly observed.[25] Although the presence of functional groups may exist from an oxidizing acid purification treatment,[29] the extremely weak D-Band (∼1320 cm^{-1}) in the Raman spectra for both purified L- and A-SWNTs is evidence for a high degree of crystallinity and relatively few defects related to functionalization in carbon nanotubes.[25,39] Further analysis of the diameter distributions was made with a complementary Ar laser at 2.54 eV for the purified laser and arc-SWNTs (see Figure S2 in the Supporting Information).

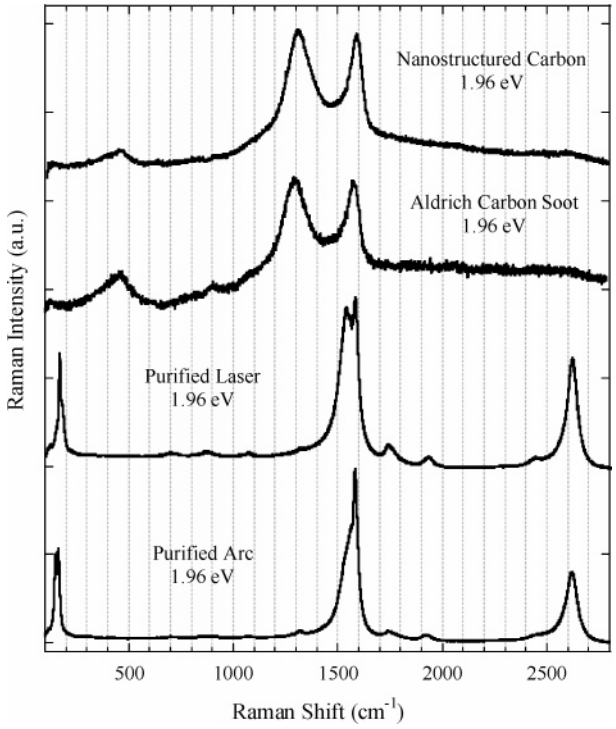

Figure 2. Overlay of the Raman spectra for nanostructured carbon (NC), carbon soot (CS-Aldrich), purified L-SWNTs, and purified A-SWNTs at an incident laser energy of 1.96 eV.

Using an expression for bundled SWNTs, the corresponding diameter distributions were calculated to range from 1.2 to 1.5 nm for laser and 1.3−1.6 nm for arc.[40] Thus, these samples exhibit a slight difference in the diameter distribution while still containing both semiconducting and metallic types.[26] Overall, based on the microscopic and spectroscopic data, the NC and CS show similar sample morphology and are appropriate representations of carbon impurities (i.e., 0% SWNT samples) for laser and arc-discharge synthesis strategies, respectively. Likewise, the purified L- and A-SWNTs represent a high degree of carbonaceous purity and are further denoted as the "100%" SWNT samples[41] for each synthesis' constructed sample set.

Constructed sample sets were prepared as previously described by volumetric mixing of stock DMA dispersions of purified SWNTs ("100%") with the respective carbon impurity constituent (NC for laser and CS for arc). However, it should be noted that the choice of carbon impurities will affect the constructed sample sets. Selection of NC is a highly suitable material since it was manufactured in the same laser synthesis reactor. Since an equivalent carbon impurity is currently unavailable from the raw arc SWNT soot vendor, the selection of CS as the most appropriate choice for a representative material has been made because it was produced under similar conditions, albeit from a different vendor. The concentration calculations for the DMA dispersions included adjustment from decomposition residue values from the TGA data such that the resulting 2.5 μg/mL is indicative of the carbonaceous content in the solutions. Figure 3 displays the characteristic optical absorption data for the DMA dispersions over the solvent transmittance window of 0.90 to 4.25 eV. Evident from the data are the well-resolved peaks due to the electronic transitions associated with the Van Hove singularities in the density of states for SWNTs.[26] The two prominent peaks at ∼1.2 and ∼1.7 eV originate from the second interband transitions of semiconducting SWNTs ($^{S}E_{22}$) and first interband transitions of metallic SWNTs ($^{M}E_{11}$), respectively.[26,42] The overall absorption in a

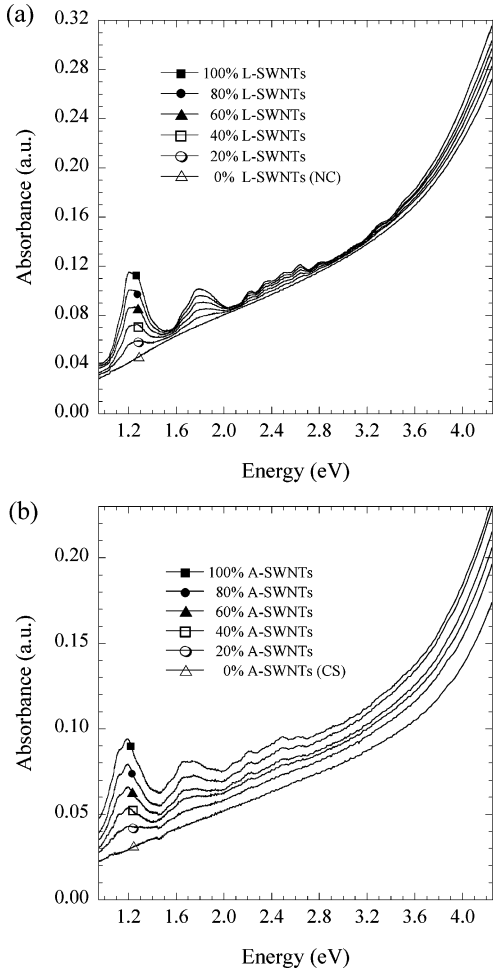

Figure 3. Optical absorption spectra for constructed sample sets of 2.5 μg/mL DMA dispersions for (a) purified L-SWNTs and NC and (b) purified A-SWNTs and CS. The data for each sample set depict the highly resolved peaks which are due to the interband electronic transitions associated with the Van Hove singularities in SWNTs.

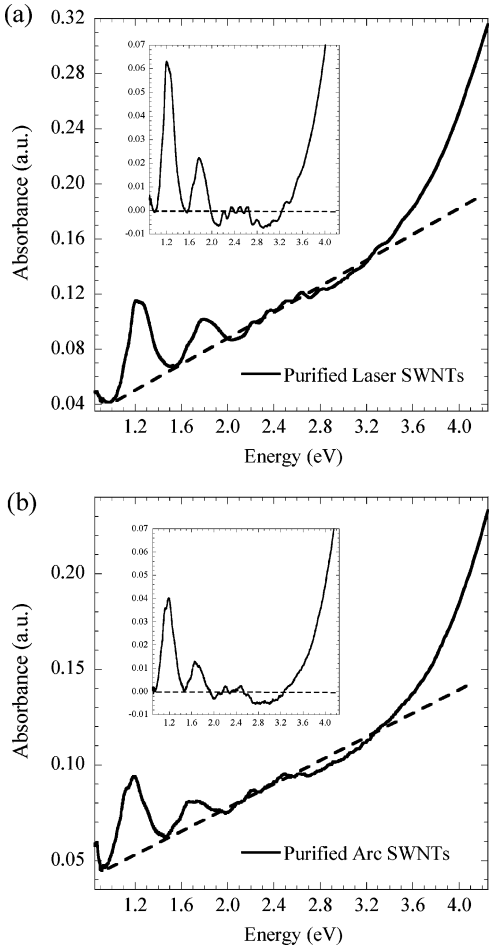

Figure 4. Optical absorption spectra for 2.5 μg/mL DMA dispersions of (a) purified L-SWNTs and (b) purified A-SWNTs. The dashed line depicts a linear extrapolation of the two minima corresponding to the $^{S}E_{22}$ peak. The insets show the resulting spectra after linear subtraction of the $^{S}E_{22}$ peak based on the extrapolated line.

SWNT-containing sample is a superposition of absorbances due to the interband electronic transitions and background π-plasmons of both the SWNTs and carbon impurities. The dramatic change in absorption intensity as a function of $^{c}w_{SWNTs}$ for both sample sets provides the necessary reference standard for comparison of purity assessment methods.

Linear Subtraction Approach. Recent attempts at purity assessment have utilized a linear subtraction over selected spectral cutoffs to estimate the absorption from non-SWNT electronic transitions for a SWNT-containing sample.[19,29−31,33,43] Application of the method reported in ref 19 to the current purified SWNTs shows a calculated areal reference ratio for purified laser SWNTs of 0.319 and for purified arc SWNTs equal to 0.253 (see Figure S3 in the Supporting Information). These values are dramatically larger than the reported value of 0.141 for the high-purity arc reference sample or the purified sample (EA-P2[33] = 0.186), further supporting the quality[43] of the purified SWNTs used in this study. The selection of the dispersion solvent (DMA instead of DMF) cannot be attributed as the main factor in these differences since the extinction coefficients for SWNTs calculated for each solvent vary by less than 2%.[28] Although the constructed sample sets do support the qualitative notion that the peak intensity at $^{S}E_{22}$ is directly related to the SWNT purity, propagation of a linear subtraction beyond the spectral cutoffs fails to accurately reflect the underlying absorption due to the SWNT π-plasmon and other carbonaceous absorption features (see Figure 4). Application of the areal ratio of the linearly subtracted $^{S}E_{22}$ peak to the total area over selected spectral cutoffs (0.97−1.53 eV for laser and 0.94 −1.47 eV for arc) for the constructed sample sets significantly deviates from the designed fractions. Shown in Figure 5 and represented by the closed data points (values are in Table 1) are the calculated SWNT fractions for both laser and arc sample sets using the current reference ratios (0.319 for purified laser and 0.253 for purified arc) as a function of the constructed SWNT mass fraction, $^{c}w_{SWNTs}$. It is apparent from the experimental results for two different SWNT chirality distributions that the reported method in ref 19 overestimates the actual SWNT fraction.

The reason for the incorrect expression in refs 19 and 29−33 for SWNT purity evaluation was also identified analytically. A complete derivation is provided as Figure S4 in the Supporting Information. The final result is represented by eq 1, which shows that the observed overestimation is based on the calculated SWNT mass fraction ($\phi_{Ref.AA}$ = eq 1 in ref 19) equaling the product between the actual mass fraction of an unknown SWNT sample (ϕ) and a ratio of total reference areal absorbance [$^{(T,R)}$AA($^{S}E_{22}$)] with the total unknown areal absorbance [$^{(T,X)}$AA($^{S}E_{22}$)] (see Figure S4).

$$\phi_{Ref.AA} = \phi\left(\frac{^{(T,R)}AA(^{S}E_{22})}{^{(T,X)}AA(^{S}E_{22})}\right) \quad (1)$$

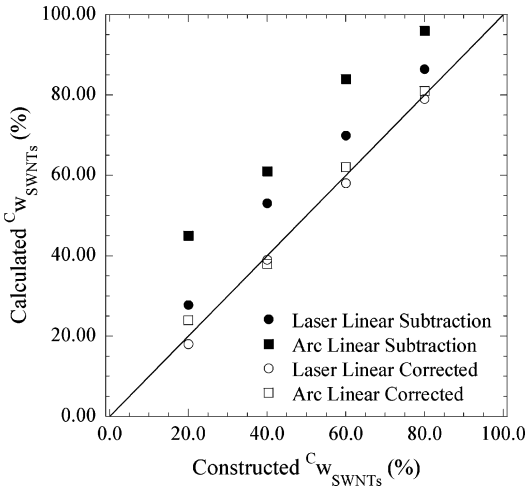

Figure 5. Purity assessment results on the constructed sample sets shown in Figure 4 for a $^{S}E_{22}$ linear subtraction with the ratio of areal absorbance to the purified SWNT reference. The closed data points represent the purity assessment results using the equation in ref 19 while the open data points are the corrected values using eq 1. The straight line represents the expected purity values for the constructed fractions of SWNTs represented in the carbonaceous mass fraction ($^{C}w_{SWNTs}$).

Since the extinction coefficient of the SWNTs is greater than that of the carbonaceous impurities, it follows that $^{(T,R)}AA(^{S}E_{22}) > {}^{(T,X)}AA(^{S}E_{22})$. Thus, the calculated value for the weight fraction of SWNTs using ($\phi_{Ref.AA}$) will always overestimate the actual value. It is important to note that the relative error will increase with decreasing values of $^{(T,X)}AA(^{S}E_{22})$, which corresponds to increasing error with decreasing SWNT purity in a sample (X-SWNT). It can also be shown with this derivation that the normalization factor resulting from division of the total area under the curve for the same spectral limits, which allows for a concentration independent measurement, introduces the described errors. Clearly, there are significant inaccuracies associated with use of the reference method,[19] demonstrated graphically in Figure 5 and mathematically in eq 1, which result in an overestimation of the actual SWNT purity level.

The suggestion in refs 19 and 29−33 that the areal peak region of a SWNT sample is proportional to the maximum areal peak region of a 100% SWNT can be a valid approach (see Figure S4). Using a modified linear peak ratio, it is possible to estimate the relative purity of SWNTs at equal solvent dispersion concentrations. The modified linear ratio calculation involves dividing the area of the peak region above the linear fit for an unknown SWNT sample [$^{(P,X)}AA(^{S}E_{22})$] by the established reference value for a pure sample [$^{(P,R)}AA(^{S}E_{22})$]. As pointed out in Figure S4, the procedure for the modified linear approach uses the peak region above the linear fit for the sample. In the present work, since the constructed samples are at equal concentrations, 2.5 μg/mL, the modified linear ratio can be applied and the results are represented by the open data points (values are in Table 1) of Figure 5. The reference values for the modified linear peak areas of the purified laser and purified arc SWNT samples are shown in Table 1 as the "100%" samples. The average percent deviation is <7% in all cases, but the average percent error increases significantly with lower SWNT designed fractions. Since selection of the spectral cutoffs for integration is based on the SWNT reference sample, the limitations associated with any linear approach are problematic, including overlap of electronic transitions and peak minima shifting from absorption of impurities in the unknown SWNT samples. Such effects are proposed to account for the higher average percent errors in the calculation at low SWNT concentrations. For a more accurate SWNT purity assessment, knowledge of the underlying contributions from the electronic transitions and π-plasmons of all constituents (i.e. SWNTs and carbonaceous impurities) is warranted. In addition, the development of a rapid assessment protocol that is concentration independent is also desirable, since the modified linear approach requires equal dispersion concentrations for proper analysis.

Nonlinear Subtraction Approach. In a given SWNT-containing sample, the total absorption at a selected energy will be a superposition of intensities from interband electronic transitions and the π-plasmon for each carbonaceous constituent. If the total π-plasmon contribution can be subtracted from the optical absorption spectrum, the resulting data will reflect only the interband electronic transitions of the SWNT materials. Therefore, appropriate modeling of the π-plasmon background and the subsequent data subtraction will enable the development of calibration curves that directly relate to the relative concentrations of each carbonaceous component. Based on these calibration curves, it is expected that a simple relationship for measuring the SWNT purity can be obtained. In comparison to a linear subtraction approach, the nonlinear function would account for physical properties in the SWNT absorption spectrum like peak overlap and transition broadening, which cannot be adequately accounted for by selection of integration limits at neighboring peak minima.

Although the underlying π-plasmon over the SWNT absorption range has been previously approximated by a linear relationship,[19,29−33] various theoretical and experimental reports have investigated the nonlinear functional dependence of this transition.[44−53] The π-plasmon is the collective excitation of the electrons associated with the π-band in a sample.[53] The peak maxima of the dispersion relation, which corresponds to the π-plasmon resonance energy (ω_π for $\hbar = 1$), are generally reported in the range of ~4.5−7 eV.[34,46,51−53] The use of a Lorentzian function to model a wide variety of physical observables involving resonance behavior is well established.[38,51] Furthermore, surface plasmons can be modeled by a driven damped harmonic oscillator, whose solution is indeed a Lorentzian in the underdamped regime.[54] Therefore, we have selected a Lorentzian function to model the carbonaceous π-plasmon in the following form:

$$L(x) = \frac{a}{1 + \left(\frac{x-b}{c}\right)^2} \qquad (2)$$

In eq 2, a is the peak amplitude, b equals the peak energy, and c is a measure of the peak width. Analyses were performed with the Kaleidagraph software package.

Lorentzian Curve Fitting Results. In the case of the constructed sample sets, the position of the π-plasmon peak is outside the solvent transmission window for DMA. Therefore, validation of the Lorentzian functional form's efficacy in fitting the π-plasmon peak was initially made by applying eq 2 to an acetone sprayed sample of purified SWNTs[28] where the peak is observable. Figure 6 shows the Lorentzian curve fit to the optical transmission data in the peak region of 4.0−5.0 eV, for the purified L-SWNT sample (see Table S1 for curve fitting parameters). The observed correlation between the curve fit and data substantiates the selection of a Lorentzian for modeling of the π-plasmon. However, it is inappropriate to use the calculated curve fitting parameters from this fit, including the peak value of ~4.5 eV, in other non-acetone sprayed samples, especially for the SWNT−DMA dispersions. This assertion is based on major differences in experimental acquisition conditions. The

TABLE 1: Purity Assessment Results for the Constructed SWNT Sample Sets Based on the Nonlinear Lorentzian Estimation of the π-Plasmon for SWNTs in a 2.5 μg/mL DMA Dispersion As Compared to the Areal Absorbance Method from the Literature and the Modified Linear Subtraction[a]

designed fraction ${}^{C}w_{SWNTs}$	Itkis et al.[19]	modified linear ${}^{S}E_{22}$	modified linear ${}^{M}E_{11}$	π-sub. ${}^{S}E_{22}$	π-sub. ${}^{M}E_{11}$
100% laser	ref 0.319[b]	ref 0.0143[b]	ref 0.00615[c]	101 (1)	103 (3)
80% laser	86 (8)	79 (1)	81 (1)	80 (0)	79 (1)
60% laser	70 (17)	58 (3)	61 (2)	59 (2)	58 (3)
40% laser	53 (33)	39 (3)	43 (8)	39 (3)	39 (3)
20% laser	28 (40)	18 (10)	24 (20)	20 (0)	19 (5)
av % dev (av rel % error)	9 (24)	2 (4)	2 (8)	1 (1)	2 (3)
100% arc	ref 0.253[d]	ref 0.00974[d]	ref 0.00370[e]	104 (4)	106 (6)
80% arc	96 (20)	81 (1)	84 (5)	78 (3)	76 (5)
60% arc	84 (40)	61 (2)	63 (5)	59 (2)	57 (5)
40% arc	61 (53)	38 (5)	50 (25)	35 (13)	36 (10)
20% arc	45 (125)	24 (20)	30 (50)	22 (10)	22 (10)
av % dev (av rel % error)	22 (59)	2 (7)	7 (21)	3 (6)	4 (7)
raw laser	31	22	28	24	30
raw arc	31	22	22	19	26

[a] The values in parentheses represent the average relative percent error for a measured fraction, ${}^{C}w_{SWNTs}$. [b] Integration limits = 0.97−1.53 eV. [c] Integration limits = 1.53−2.08 eV. [d] Integration limits = 0.94−1.47 eV. [e] Integration limits = 1.47−2.00 eV.

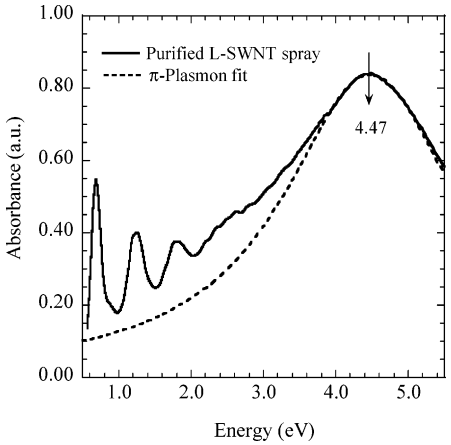

Figure 6. Optical absorption spectra of purified L-SWNTs sprayed onto a quartz slide from a 0.1 mg/mL of acetone solution with the corresponding nonlinear π-plasmon curve fit shown by the dashed line. The Lorentzian curve fit from the data between 4.0 and 5.0 eV shows a strong correlation to the peak region of the data, and the peak maxima denoting the π-plasmon energy is calculated to be 4.47 eV.

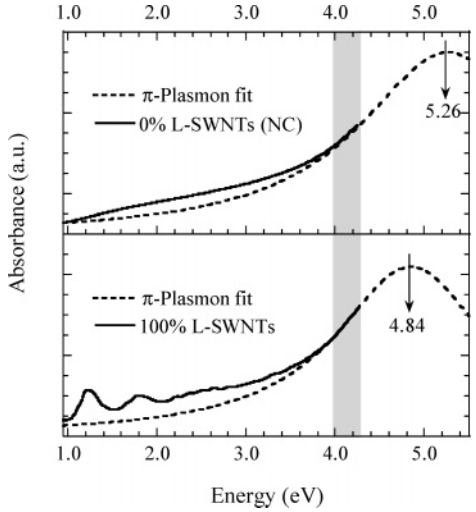

Figure 7. Optical absorption spectra of 2.5 μg/mL DMA dispersions of 0% L-SWNTs (NC) and 100% L-SWNTs with the corresponding nonlinear π-plasmon curve fits shown by dashed lines. The peak maximum denoting the π-plasmon energy is calculated to be 4.84 eV for the 100% L-SWNTs and 5.26 eV for the 0% L-SWNTs (NC). The gray band depicts the data region from which the nonlinear π-plasmon curve fit was generated.

effects of SWNT bundling,[55] solvent interactions during dispersion,[56] or thin film particle scattering in the sprayed sample[36] are several examples of these differences. Instead, the Lorentzian curve fits for the constructed sample sets were generated from the optical absorption data between 4 and 4.25 eV, where the π-plasmon absorption is proposed to be dominant in comparison to the electronic transitions of the carbonaceous materials. The resulting curve fits are shown for the DMA dispersions containing purified L-SWNT, A-SWNT, NC, and CS in Figures 7 and 8. The Lorentzian curve fits for the purified SWNTs are expected to represent the superposition of π-plasmon contributions from the entire distribution of SWNT diameters and electronic types present in each sample. Similarly, the Lorentzian curve fits for NC and CS are a superposition of the π-plasmon contributions from the various carbonaceous components, including the overall morphology and particle sizes in each sample. There is a strong correlation between the optical absorption data and chosen Lorentzian functional form (see Figure S5 in the Supporting Information). A summary of the fitting parameters (R^2 exceeding 0.999 for each over the prescribed data range of 4.00−4.25 eV) for the L- and A-SWNTs, NC, and CS is provided in Table S1 in the Supporting Information. Sensitivity of this approach to the range of data for curve fitting was also investigated, but the most reasonable agreement with the spectral features of the SWNTs was observed for the prescribed data range. Slight variations in the fitting region (e.g., 3.75−4.00 and 3.75−4.25 eV) resulted in little or no change in the low energy range (~1−2 eV) where the purity assessment is performed. The value of the Lorentzian curve fits at 1.5 eV showed a deviation of less than 5% for the data ranges examined. Therefore, the Lorentzian function was deemed an appropriate approximation to the π-plasmon for the constructed sample sets.

The Lorentzian curve fits determined the π-plasmon resonance energy to be at 4.84 eV for the purified L-SWNTs and 4.90 eV for the purified A-SWNTs. As expected, the location of the π-plasmon peak positions has shifted between sprayed solid sample and solvent dispersion due to the differences in experimental conditions. However, the measured and projected

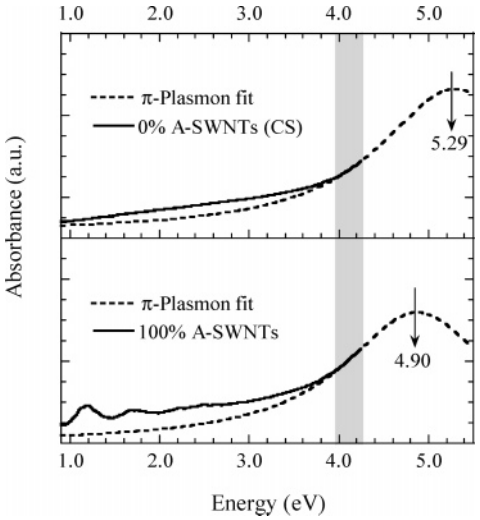

Figure 8. Optical absorption spectra of 2.5 μg/mL DMA dispersions of 0% A-SWNTs (CS) and 100% A-SWNTs with the corresponding nonlinear π-plasmon curve fits shown by dashed lines. The peak maxima denoting the π-plasmon energy is calculated to be 4.90 eV for the 100% A-SWNTs and 5.29 eV for the 0% A-SWNTs (CS). The gray band depicts the data region from which the nonlinear π-plasmon curve fit was generated.

values are consistent with experimental reports using optical absorption spectroscopy of evaporated SWNTs where the peak was stated to be "around 5 eV". [51] Previous work with electron energy loss spectroscopy (EELS) has resulted in a slightly higher ω_π equal to 5.2 eV.[53] The nonlinear curve fit values also suggest that the $\pi-\pi$ overlap integral, γ_o, which can be approximated as $\omega_\pi/2$,[49] is equal to ~2.45 eV for the purified SWNT−DMA dispersions. (Identification of γ_o is an important parameter for calculating the interband electronic transitions unique to the individual SWNT diameters, and would specifically aid in the deconvolution of the optical absorption spectra based on the energy band calculations.)[26,57−59] The curve fits for the π-plasmons of NC (ω_π = 5.26 eV) and CS (ω_π = 5.29 eV) show a general trend whereby the resonance energy is higher than that for the purified SWNTs in the DMA dispersions. This would be consistent with a lowering of the energy required for the collective $\pi-\pi^*$ transitions in SWNTs since the highly conjugated π-system leads to delocalization of the electrons.[56] The absorption of C_{60} fullerenes that occurs at 3.7 eV is below the employed curve fit range, but may influence the curve fitting approach if significant quantities are present. Since in both NC and CS the presence of C_{60} was low (~3% w/w), consistent with the lack of any spectral signature, the contribution to the curve fit is considered negligible.

In the constructed sample sets, the Lorentzian curve fits are a superposition of all the π-plasmon contributions present in the sample, including both SWNT and carbonaceous impurity distributions. The resulting nonlinear π-plasmon functions showed similar curve fitting parameters for both laser and arc constructed sample sets. The expected trend of increased peak energy with a decrease in the designed SWNT fraction (see Table S1 in the Supporting Information) was observed. The resulting optical absorption spectra, after subtraction of the nonlinear π-plasmon functions, are shown in Figure 9 for both constructed sample sets. It is important to note that any effects due to particle scattering in the DMA dispersions, which have previously been reported as negligible for DMF and aqueous dispersions at higher concentrations,[19,36] may be used as a further refinement to the ascribed nonlinear subtraction. The data indicate a broad absorption over the energy range for both NC

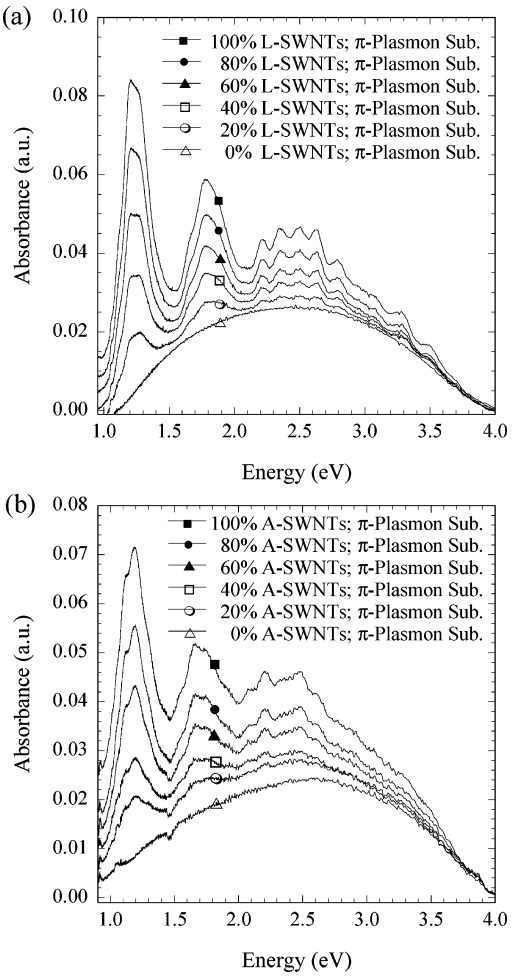

Figure 9. Optical absorption spectral overlays for nonlinear π-plasmon subtractions of the constructed sample sets for (a) L-SWNTs and (b) A-SWNTs.

and CS materials which are attributed to the electronic transitions of the constituent carbonaceous materials (such as fullerenes, amorphous carbon, and other graphitic components).[38,60] The purified L-SWNTs and A-SWNTs display well-resolved peak structures, particularly in the region above 2 eV, representative of the electronic transitions for each diameter and electronic type. Such spectra are expected to enable the appropriate deconvolution of absorption data based the predicted energy gap transitions for individual SWNT diameters.[26] This type of analysis will allow for the calculation of the semiconducting: metallic ratio (S:M) for any SWNT diameter distribution and serve as a means for accurate assessment of electronic type separations.[61]

An observed result from the nonlinear curve fits is that the minima between peaks ($^SE_{22}$ and $^ME_{11}$ for example) do not equal zero. This result is consistent with the expectation that an optical absorption spectrum of SWNTs exhibits an overlap of electronic transitions and peak broadening for individual transitions. Such physical properties are not accounted for in a linear subtraction model, and are important factors in determining an appropriate π-plasmon subtraction. Overlap of electronic transitions may exist due to variation in the density of states for the collection of diameters and chiralities involved with the optical absorption. Therefore, with the typical diameter distribution ranging from 1.2 to 1.5 nm for laser (1.3−1.6 nm for arc), the possibility exists that an optical absorption peak from a smaller diameter semiconducting SWNT could overlap with a larger diameter metallic SWNT. In addition, peak broadening in the case of

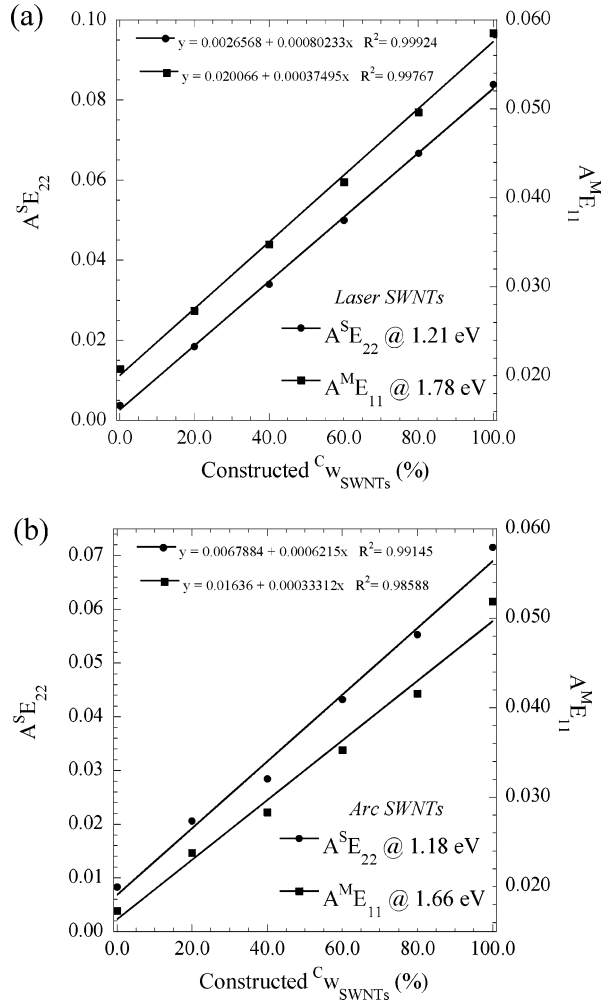

Figure 10. Calibration curves for purity assessment from the nonlinear π-plasmon subtracted constructed sample sets for (a) L-SWNTs and (b) A-SWNTs. The data were selected from the peak energy values in Figure 9 associated with the maximum absorbance at $^{S}E_{22}$ and $^{M}E_{11}$ for each constructed fraction.

SWNTs could be influenced by structural distortions and defects, finite SWNT lengths, or bundling effects[55] arising from the van der Waals interactions between SWNTs. Although the SWNTs in the DMA dispersions have been proposed to be debundled compared to the bulk purified material,[28] there is currently no evidence to support that all species exist as individual SWNTs. Improvements in assessment protocols may allow for investigation of these features, including a refined model that identifies the precise nature of SWNT bundling properties.

Calibration Curves for Purity Assessment. Each of the designed fractions in Figure 9 coincides with the appropriate superposition of absorbance expected from the constructed dilutions between NC (CS) and L-SWNTs (A-SWNTs). Therefore, it is possible to establish calibration curves for both laser and arc SWNTs utilizing the constructed sample sets. Figure 10 demonstrates the linear relationships that result from selection of the absorbance values at the peak maxima for the semiconducting ($A^{S}E_{22}$) and metallic ($A^{M}E_{11}$) transitions in both constructed sample sets. The anticipated correlation between the data and the linear curve fit is clearly observed. The calibration lines are unique to the SWNT constructed sample sets from Figure 9 and therefore cannot be used as an absolute metric for material comparison with any SWNT sample or diameter distribution. Development of such calibration curves is also relative to the initial choice of carbon impurity used to fabricate the constructed sample sets (NC for laser and CS for arc). The results, however, clearly demonstrate the methodology for SWNT purity assessment of typical laser and arc-synthesized materials. Future work will evaluate the robustness of these calibration lines based on various carbon impurities and SWNT distributions, but is beyond the scope of this report.

There are important considerations related to the choice of analysis used to generate the calibration curves (i.e., peak maxima versus integrated peak area). In the present case, the use of peak maxima values has important advantages over integrated area based on the observed SWNT distribution. For the laser and arc $^{S}E_{22}$ and $^{M}E_{11}$ peaks in Figure 9, the superposition of interband electronic transitions based on the samples' diameter ranges give rise to a peaked distribution with the amplitude proportional to the area with minimal effects of peak overlap (as described above) and appropriate selection of integration limits. The degree of overlap is largely influenced by the type of SWNT distribution being evaluated, since the density of interband electronic transitions over a particular energy range dictates this overlap as visualized from a Kataura plot.[26] In samples where the interband peaks result in multimodal structures and selection of integration limits is less problematic, then the integrated area approach may prove worthwhile.

Application of the calculated linear trendlines in Figure 10 is specific to 2.5 μg/mL DMA dispersion, but this approach is valid for any concentration below the dispersion limit. The purity assessment results as seen in Table 1 are dramatically improved compared to the reported areal absorbance ratio method[19] and consistently show better correlation with the lower designed SWNT mass fractions than the modified linear subtraction. The calculated fractions using the nonlinear π-plasmon subtraction are within an average deviation of the designed values by 1−2% for the L-SWNTs and 3−4% for the A-SWNTs. In comparison, the modified linear subtraction has a slightly higher deviation of 2−7% depending on the SWNT sample and selected peak, and the method in ref 19 corresponds to 9% for L-SWNTs and 22% for A-SWNTs. Another consideration is the accuracy of the calculated value to the designed value, represented by the average relative percent error shown in parentheses in Table 1. For the nonlinear π-plasmon subtracted approach, the L-SWNTs exhibit an average relative error within 3% of any designed fraction and the A-SWNTs are within 7% for either peak. The modified linear subtraction shows relatively good agreement for the $^{S}E_{22}$ peaks in the laser and arc sample sets, but shows significantly higher average relative errors from the $^{M}E_{11}$ peak. The method in ref 19, however, is at best within an average relative error of 24% for laser and 59% for arc-SWNTs.

Modifications in the SWNT diameter distributions and (S:M) may alter the empirical calibration curves, but the nonlinear curve fitting approach has demonstrated success for both laser and arc SWNTs. The natural extension of these results from the constructed sample sets is to evaluate raw laser and arc SWNT soots with the established nonlinear π-plasmon fit and calibration curves. Shown in Figure 11 are the optical absorption spectra for 2.5 μg/mL DMA dispersions of raw L- and A-SWNT soots, including the corresponding Lorentzian curve fits for the raw soots. The π-plasmon subtracted data are depicted in the insets for both L-SWNT and A-SWNT soots with the corresponding "0%" and "100%" SWNT subtracted spectra also shown as a reference for comparison. In the acquired data, there is a slight increase in the absorption of the raw laser soot as compared to the purified spectra between ~2 and 3 eV evident by the offset in the overlay. This increase in absorption

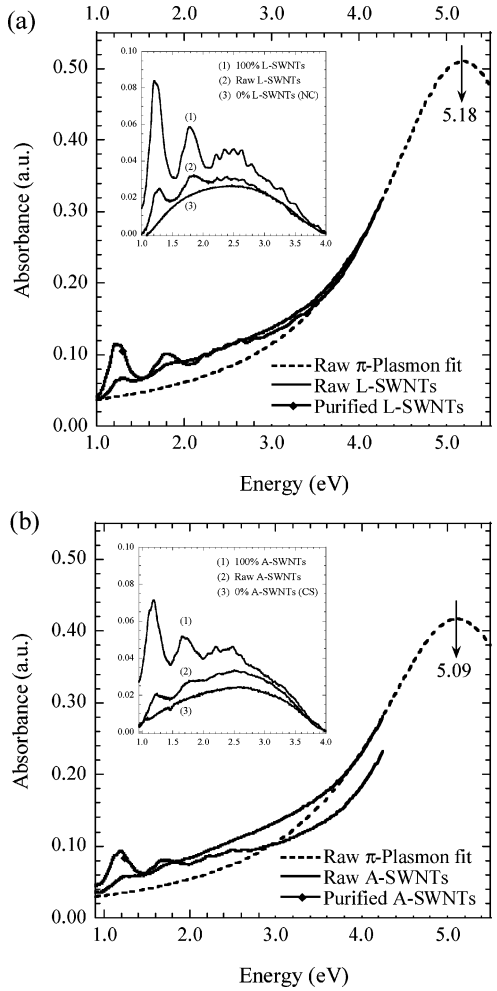

Figure 11. Optical absorption spectra of 2.5 μg/mL DMA dispersions for (a) raw L-SWNTs and (b) raw A-SWNTs (as-purchased from Carbon Solutions, Inc.). The corresponding nonlinear π-plasmon fits for the raw SWNTs are represented by the dashed lines. The spectra for purified SWNTs from each synthetic type are also overlaid for reference. The insets compare the π-plasmon subtracted results for each raw SWNT soot against the 0% and 100% SWNT samples for each synthetic type.

is proposed to result from the carbonaceous coatings that are produced during synthesis and are removed during the high-temperature oxidation treatments in the purification. It is expected that the carbonaceous coatings will have an effect on the observed π-plasmon energy, and indeed there are differences between the raw SWNT soots and the expected values from the constructed sample sets (see Table S1). The offset is more dramatic in the case of the raw arc soot, thereby suggesting that the degree of carbonaceous coatings would be higher. However, the raw arc soot may have originally contained graphitic material (see high-temperature TGA decomposition results in Figure S1). The possibility then exists that the purified A-SWNTs has retained this graphitic constituent since the purification process may not be efficient at its removal. The effects of C_{60} and other fullerenes can also impact the optical absorption data of raw SWNT soot, but current results from a toluene extraction of the raw laser and raw arc materials show only trace quantities (<1% w/w). Therefore, the higher absorption in this range is likely a combination of effects in the raw soots, but does not significantly impact purity assessment through analysis of the $^{S}E_{22}$ peak. The data indicate that the $^{S}E_{22}$ peak is most accurate due to confounding effects of carbonaceous coatings from synthesis. The results using the

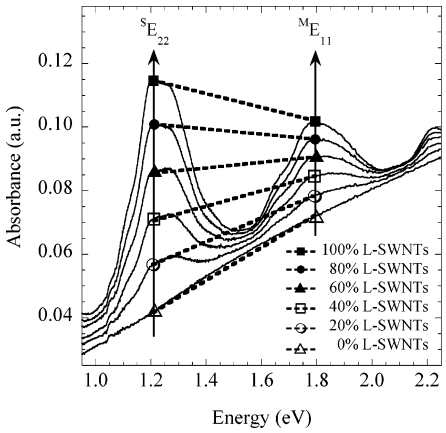

Figure 12. Optical absorption spectra from Figure 3a for the constructed L-SWNT sample set where the peak maxima for the $^{S}E_{22}$ and $^{M}E_{11}$ transitions are highlighted with the symbols. The dashed tie line, which is drawn between the peak maxima, indicates the relative changes in slope of this line between peaks for each SWNT fraction.

calibration curves for the $^{S}E_{22}$ peak in Figure 10 on the π-plasmon subtracted raw SWNT soot data are shown in Table 1. The raw L-SWNT soot and A-SWNT soot were calculated to equal 24% w/w and 19% w/w SWNTs of the total carbonaceous material, respectively. As expected, these values are substantially lower than the calculated 31% for both laser and arc based on the areal absorbance ratio method using the current reference ratios (0.319 for purified laser and 0.253 for purified arc). However, the modified linear subtraction is relatively consistent with the π-plasmon subtracted results indicating a value of 22% w/w for each raw SWNT soot. When the TGA data (raw L-SWNT soot residue = 10.2% and raw A-SWNT soot residue = 31.9% w/w) are accounted for, the resulting total mass fraction from the π-plasmon subtraction results is 22% w/w for raw laser and 13% w/w for raw arc. These values are strikingly lower than previous reports,[19,29,30,35] but are consistent with the microscopic analysis in Figure 1.

Rapid Purity Assessment Protocols. While the nonlinear π-plasmon model has been demonstrated as a physically robust approach, the generation and implementation of calibration curves are not time efficient for large number of samples and do not allow for critical evaluation of results in presentations or publications without access to the actual data. Therefore, it is also desirable to establish rapid assessment protocols which facilitate SWNT sample screening during synthesis, purity monitoring during purification procedures, and enable the estimation of purity from visual observation during presentations or in publications. Based on the constructed sample sets, there are several important observations which can be incorporated into purity assessment protocols. As shown in Figure 12, the absolute intensity and ratio of intensities of the $^{S}E_{22}$ peak and $^{M}E_{11}$ peak for the L-SWNT constructed sample set (as well as for the A-SWNT constructed sample set) varies consistently with the relative weight fraction of SWNTs present. Further visualization can be made by drawing tie lines from peak maxima and observing the changes in slope of the line as a function of weight fraction. Therefore, such observations present alternative strategies for SWNT purity assessment.

Both laser and arc constructed sample sets were evaluated based on a summation of the absorbance values for the $^{S}E_{22}$ and $^{M}E_{11}$ peaks as a function of the designed SWNT fraction. The results are shown in Figure 13a and illustrate the linear relationship for both cases which are normalized to dispersion concentration (i.e., absorbance values were divided by the

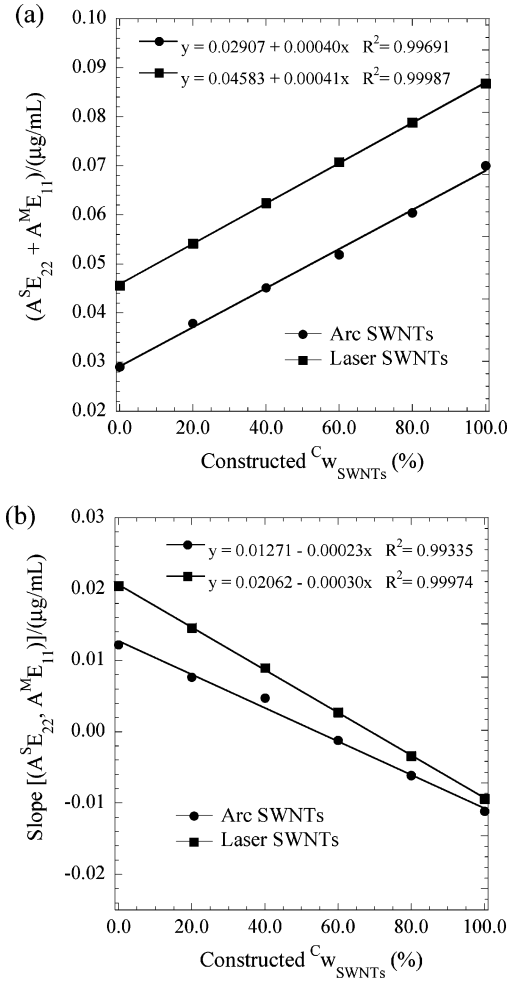

Figure 13. Rapid purity assessment methods on L-SWNT and A-SWNT constructed sample sets using the (a) peak sum of the absorbance maxima at $^{S}E_{22}$ and $^{M}E_{11}$ and (b) slope from the tie lines between absorbance maxima at $^{S}E_{22}$ and $^{M}E_{11}$. The linear curve fits indicate the empirical relationships for each method and SWNT synthesis type. The data sets have been normalized to 1 μg of SWNTs/mL of DMA.

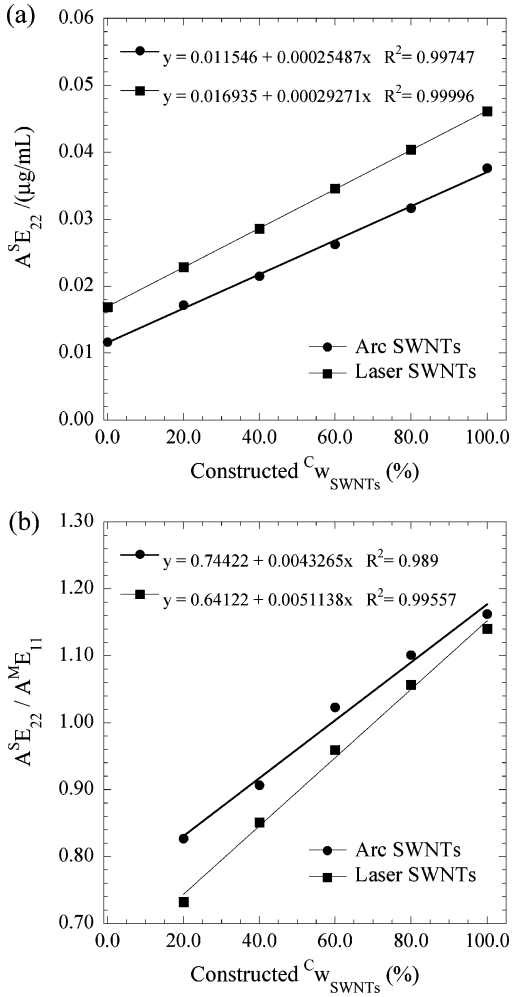

Figure 14. Rapid purity assessment method on the L-SWNT and A-SWNT constructed sample sets using the (a) maximum absorbance value for the $^{S}E_{22}$ peak normalized to 1 μg of SWNTs/mL of DMA and (b) the ratio of absorbance values for the $^{S}E_{22}$ and $^{M}E_{11}$ peaks. The linear curve fits indicate the empirical relationships for each method and SWNT synthesis type.

dispersion concentration of 2.5 μg/mL). The offset in *y*-intercepts is attributed to the differences in the maximum absorption which can result from different extinction coefficients (SWNT or selected carbon impurities), SWNT molecular weights, or purity between purified L- and A-SWNTs. (Such an offset in the absorption for purified A-SWNTs can be related to any residual graphite in the sample, thereby altering the DMA dispersion concentration during analysis.) Evaluation of the slope for peak maxima tie lines also results in a linear trendline as depicted in Figure 13b. The data are also normalized to dispersion concentration and show a convergence of maximum negative slope (approaching −0.012) for the "100%" sample in both laser and arc constructed sample sets. An interesting observation from this plot is that for peak maxima tie lines of *zero* slope, the purity is approximately *70% w/w SWNTs* in the carbonaceous component. This result implies that positive tie line slopes will occur for samples of less than 70% w/w SWNTs and negative slopes exist for samples of greater purity. Comparison of the peak maxima summation or tie line slope for a sample with unknown SWNT purity to the empirical relations (normalized to the dispersion concentration of 1 μg/mL) in Figure 13 will allow for the rapid determination of its carbonaceous purity.

The $^{S}E_{22}$ peak was previously shown to be least affected by the absorption from the carbon impurities in a sample (Figure 9), and from the carbonaceous coatings (Figure 11), therefore the use of this peak for a rapid assessment method is plausible and simple. Shown in Figure 14a are the data for the absorbance value of the $^{S}E_{22}$ peak for both L-SWNT and A-SWNT constructed sample sets normalized to dispersion concentration. The resulting linearity represents a simple and straightforward method to rapidly assess SWNT purity. A linear dependence is also observed when the ratios of peak maximum absorbance values were plotted as shown in Figure 14b. Both constructed sets of purified SWNT samples exhibit a peak maxima ratio approaching 1.2 in the plot. A similar observation to the slope approach is that for a ratio ($A^{S}E_{22}/A^{M}E_{11}$) of *1.0* (corresponding to a zero tie line slope), the purity of a given sample is approximately *70% w/w SWNTs* in the carbonaceous component. Therefore, the same notion exists where peak maxima ratios greater than 1.0 will occur for samples greater than 70% w/w SWNTs and ratios lower than 1.0 exist for purity levels less than 70% w/w SWNTs. In comparison to the other rapid assessment methods, the peak maxima ratio is extremely attractive since it is independent of the dispersion concentration (i.e., the concentration terms cancel upon division), provided the dispersion being analyzed is below the SWNT-solvent dispersion limit. The ratio of peak absorbances can result in an important derivation (eq 3) whereby convolution of the purity

TABLE 2: Calculated Extinction Coefficients of SWNTs, NC, and CS in DMA Dispersions at Selected Energies for Beer's Law Analysis

solute	ϵ ($^{S}E_{22}$) (mL·mg^{-1}·cm^{-1})	ϵ ($^{M}E_{11}$) (mL·mg^{-1}·cm^{-1})
CS (Aldrich)	10.5 (1.18 eV)	16.5 (1.65 eV)
NC	15.5 (1.21 eV)	26.8 (1.78 eV)
purified A-SWNTs	35.0 (1.18 eV)	30.0 (1.65 eV)
purified L-SWNTs	45.5 (1.21 eV)	40.0 (1.78 eV)

with the (S:M) and ratio of extinction coefficients also occurs.

$$\frac{A(^{S}E_{22}) \equiv \epsilon_S l c_S}{A(^{M}E_{11}) \equiv \epsilon_M l c_M} = \left(\frac{\epsilon_S}{\epsilon_M}\right)\left(\frac{\zeta}{1-\zeta}\right) \quad (3)$$

where $c_S = \zeta c_T$ and $c_M = (1 - \zeta)c_T$. Equation 3 represents the ratio of peak maxima for a pure SWNT sample given the fact that there is no concentration term for the impurities. The variables ϵ_S and ϵ_M are the extinction coefficients for semiconducting and metallic SWNTs, respectively, l is the optical path length, c_S is the concentration of semiconducting, c_M is the concentration of metallic SWNTs, c_T is the total SWNT concentration, and ζ is the fraction of the total SWNT concentration that is semiconducting. As a result, the derivation shows that (S:M) is equal to $\zeta/(1 - \zeta)$.

If the (S:M) is assumed to remain constant (typically reported at 2:1[38,61]), then appropriate use of extinction coefficients in a Beer's law analysis yields another method for purity assessment. While overlap of SWNT electronic transitions can influence an experimentally calculated ϵ, the value derived from selecting the peak maximum will be the least sensitive to this effect. Previous work has determined the value of the extinction coefficients for NC, raw, and purified L-SWNT−DMA dispersions.[28] A similar analysis has been made using CS and purified A-SWNTs for comparison with the laser data. Shown in Table 2 are the calculated extinction coefficients derived from a Beer's law analysis involving serial dilution of the 2.5 μg/mL DMA dispersions for each material with pure DMA. These results are consistent with the previous values.[28] Since the mass used to calculate the dispersion concentrations for the Beer's law analysis was for the total concentration of purified SWNTs, c_T, the magnitude of the extinction coefficient values is a convolution of the extinction properties for the inherent (S:M). Therefore, as long as the SWNT samples being analyzed have a similar (S:M), incorporation of these constants into eq 4 will result in a relative determination of the carbonaceous concentration ratio between the total bulk SWNTs (c_T) and carbonaceous impurities (c_{CI}).

$$\frac{c_T}{c_{CI}} = \frac{[A(^{M}E_{11})\cdot\epsilon_{CI}(^{S}E_{22}) - A(^{S}E_{22})\cdot\epsilon_{CI}(^{M}E_{11})]}{[A(^{S}E_{22})\cdot\epsilon(^{M}E_{11}) - A(^{M}E_{11})\cdot\epsilon(^{S}E_{22})]} \quad (4)$$

where

$$^{C}w_{SWNTs} = \left(\left(\frac{c_T}{c_{CI}}\right)/\left(1 + \frac{c_T}{c_{CI}}\right)\right)$$

Extinction coefficients for SWNTs have been reported in the literature, but an uncertainty exists in regard to what these values represent.[32,33,62,63] Disparities in the value of the dispersion limit for the various species present in a SWNT-containing sample (i.e., SWNTs, graphitic carbon, amorphous carbon, and/or fullerenes) call into question what material is the major contributing factor to the measured extinction coefficients. (Note: The dispersion limit of nanostructured carbon is 2 orders of magnitude higher than that of the purified SWNTs in DMA.[28]) For unambiguous interpretation of any extinction coefficient data, it is imperative that measurements be performed below the dispersion limit of purified SWNTs in the solvent (e.g., ~3 μg/mL for a DMA dispersion).[28] In the future, determination of the absolute extinction coefficients for semiconducting and metallic SWNTs will greatly facilitate purity assessment, including the ability to accurately quantify the bulk degree of enrichment from SWNT separations.[61] In addition, an understanding of how the extinction coefficient may vary with SWNT diameter can elucidate the overall absorption profile further.

TABLE 3: Purity Assessment Results for the Constructed SWNT Sample Sets Based on the Rapid Protocols[a]

designed fraction $^{C}w_{SWNTs}$	$A(^{S}E_{22}) + A(^{M}E_{11})$	slope [$(A(^{S}E_{22}), A(^{M}E_{11})]$	$A(^{S}E_{22})$	$A(^{S}E_{22})/A(^{M}E_{11})$	Beer's law
100% laser	99 (1)	100 (0)	100 (0)	96 (4)	99 (1)
80% laser	80 (0)	80 (0)	80 (0)	80 (0)	79 (1)
60% laser	61 (2)	60 (0)	60 (0)	62 (3)	58 (3)
40% laser	40 (0)	39 (3)	40 (0)	40 (0)	38 (5)
20% laser	20 (0)	20 (0)	20 (0)	17 (15)	20 (0)
av % dev (av rel % error)	<1 (1)	<1 (1)	0 (0)	2 (5)	1 (2)
100% arc	103 (3)	101 (1)	102 (2)	97 (3)	99 (1)
80% arc	78 (3)	80 (0)	79 (1)	82 (3)	80 (0)
60% arc	56 (7)	59 (2)	58 (3)	64 (7)	60 (0)
40% arc	39 (3)	34 (15)	39 (3)	37 (8)	37 (8)
20% arc	21 (5)	21 (5)	22 (10)	19 (5)	24 (20)
av % dev (av rel % error)	2 (4)	2 (5)	2 (4)	3 (5)	2 (6)
raw laser	34	17	28	19	20
raw arc	53		42	9	18

[a] The values in parentheses represent the average relative percent error for a measured fraction, $^{C}w_{SWNTs}$.

In summary, the results from each of the rapid techniques on the constructed sample sets are listed in Table 3. Also included are the rapid assessment results on the 2.5 μg/mL raw laser and arc SWNT-DMA dispersions. The proposed effects of carbonaceous coatings are most apparent in the peak summation approach for both raw samples. However, the results for raw laser SWNTs are consistent across each of the techniques with only a minor depression in values compared to the nonlinear π-plasmon model. In contrast, the raw arc SWNT soot shows significantly more variability in each of the rapid assessment analyses, specifically with the slope approach where the measured value is outside the calculated calibration range. As suggested earlier, this variability is attributed to the presence of increased carbonaceous coatings or graphitic components in the arc sample that artificially inflate the absorption in the $^{M}E_{11}$ peak range, thereby altering the purity assessment results. While the peak summation and tie line slope approach are useful techniques, they are also dispersion concentration dependent, which reduces their appeal. In comparison, the peak maxima ratio ($A^{S}E_{22}/A^{M}E_{11}$) and Beer's law strategies are concentration independent, provided the SWNT-DMA dispersion is below the dispersion limit (~3 μg/mL for purified SWNTs[28]). With these observations in mind, the recommended rapid approach to purity assessment includes the following simple procedure: (1) perform TGA analysis of SWNT sample; (2) use corrected carbonaceous mass from TGA residue to prepare and analyze a 2.5 μg/mL SWNT−DMA dispersion from 0.9 to 4.25 eV, using optical absorption spectroscopy; (3) evaluate the absor-

bance peak maximum values for the $^{S}E_{22}$ and $^{M}E_{11}$ peaks; (4) calculate the peak maximum ratio and compare to the calibration curve or utilize Beer's law (eq 3) with appropriate extinction coefficients for an assessment of the $^{c}w_{SWNTs}$ in the carbonaceous component; (5) and adjust for the metal catalyst impurities from the TGA residue to determine the overall w_{SWNTs} in the analyzed sample.

Conclusion

The use of optical absorption spectroscopy on SWNT−DMA dispersions has been shown to produce highly resolved spectra which allow for a quantitative, noninvasive approach to probing the bulk SWNT electronic transitions. Production of constructed sample sets containing purified laser (arc) SWNTs with nanostructured carbon (carbon soot) has enabled the necessary verification of purity assessment methods for calculation of the carbonaceous mass fraction of SWNTs ($^{c}w_{SWNTs}$). Evaluation of the purity assessment method with use of the areal ratio from a linear subtraction has shown where this approach overestimates the actual SWNT content when a total area normalization is utilized, supported by both experimental data and a mathematical derivation. The development of a nonlinear π-plasmon regression model has been used to generate calibration curves which show minimal deviation (error <3% for laser and <7% for arc sample sets) and are able to extrapolate to SWNT samples of differing purity levels. Innovative rapid assessment protocols based on absorbance maxima, peak tie line slopes, relative absorbance ratios, and Beer's law analysis of the $^{S}E_{22}$ and $^{M}E_{11}$ peaks have been developed and corroborated with the nonlinear π-plasmon model. An important observation from the results is that for equivalent absorbance intensities of the $^{S}E_{22}$ and $^{M}E_{11}$ peaks, SWNT-containing samples are ∼70% w/w SWNTs of the carbonaceous component. These methods represent both a robust and an efficient means to accurately quantify the overall mass fraction of SWNTs in a given sample based on the appropriate combination of TGA and optical absorption spectroscopy. While the methodologies herein have been shown to be robust, the purity assessment comparisons are relative to the absolute purity of the "100%" SWNT samples and appropriate selection of carbon impurities for the constructed sample sets. As noted previously, the proposed protocols will remain valid even with samples of potentially higher SWNT purity. The generality of the calibration curves for SWNT samples with differing distributions and sample impurities is currently being investigated, including the quantification of individual diameter concentrations and the semiconducting:metallic ratio. Refinements to this approach will address the carbonaceous coatings on raw SWNT soots, chemical functionalization that can result during purification, and any residual graphite impurities that may exist from arc-discharge techniques. Overall, the improved understanding of SWNT purity assessment will assuredly lead to more accurate analyses and consistency in experimental results necessary for future device development.

Acknowledgment. The authors wish to thank Jim Worman, George Thurston, Mike Kotlarchyk, and John Andersen for helpful discussions during this work. Financial support for this project was made by BP Solar, the National Science Foundation (Grant No. ECS-0233776), Department of Energy (Grant No. DE-FG02-02ER63393), NASA (Grant Nos. NAG3-2828 and NCC3-956), and the Rochester Institute of Technology's First In Class Initiative. B.J.L. also acknowledges financial support from a NASA Graduate Student Research Fellowship.

Supporting Information Available: TGA data for the raw and purified arc-SWNTs, raw and purified laser-SWNTs, and the nanostructured carbon and carbon soot materials are shown in Figure S1; Raman spectra of the radial breathing modes for the purified laser and arc SWNTs, using the 1.96 and 2.54 eV incident laser energies, are shown in Figure S2; calculation of the areal absorbance reference ratios for the purified laser and arc SWNTs used in this study are shown in Figure S3; Figure S4 provides the appropriate derivation of the reference method[19] to mathematically show where the ratio of areal absorbances leads to an overestimation for SWNT purity assessment; the nonlinear curve fits generated from the data over the 4.00−4.25 eV range from the optical absorption spectra are shown in Figure S5; and the curve fitting parameters determined for each nonlinear curve fit are provided in Table S1. This material is available free of charge via the Internet at http://pubs.acs.org.

References and Notes

(1) Avouris, P.; Martel, R.; Derycke, V.; Appenzeller, J. *Phys. B* **2002**, *323*, 6.
(2) Dai, H. *Surf. Sci.* **2002**, *500*, 218.
(3) Landi, B. J.; Raffaelle, R. P.; Heben, M. J.; Alleman, J. L.; VanDerveer, W.; Gennett, T. *Nano Lett.* **2002**, *2*, 1329.
(4) Chiang, I. W.; Brinson, B. E.; Smalley, R. E.; Margrave, J. L.; Hauge, R. H. *J. Phys. Chem. B* **2001**, *105*, 1157.
(5) Chiang, I. W.; Brinson, B. E.; Huang, A. Y.; Willis, P. A.; Bronikowski, M. J.; Margrave, J. L.; Smalley, R. E.; Hauge, R. H. *J. Phys. Chem. B* **2001**, *105*, 8297.
(6) Dillon, A. C.; Gennett, T.; Jones, K. M.; Alleman, J. L.; Parilla, P. A.; Heben, M. J. *Adv. Mater.* **1999**, *11*, 1354.
(7) Dillon, A. C.; Gennett, T.; Parilla, P. A.; Alleman, J. L.; Jones, K. M.; Heben, M. J. *Mater. Res. Soc. Symp. Proc.* **2001**, *633*, A5.2.1.
(8) Harutyunyan, A. R.; Pradhan, B. K.; Chang, J.; Chen, G.; Eklund, P. C. *J. Phys. Chem. B* **2002**, *106*, 8671.
(9) Moon, J.-M.; An, K. H.; Lee, Y. H.; Park, Y. S.; Bae, D. J.; Park, G.-S. *J. Phys. Chem. B* **2001**, *105*, 5677.
(10) Strong, K. L.; Anderson, D. P.; Lafdi, K.; Kuhn, J. N. *Carbon* **2003**, *41*, 1477.
(11) Arepalli, S.; Nikolaev, P.; Gorelik, O.; Hadjiev, V. G.; Holmes, W.; Files, B.; Yowell, L. *Carbon* **2004**, *42*, 1783.
(12) Li, H.; Guan, L.; Shi, Z.; Gu, Z. *J. Phys. Chem. B* **2004**, *108*, 4573.
(13) Shi, Z.; Lian, Y.; Liao, F.; Zhou, X.; Gu, Z.; Zhang, Y.; Iijima, S. *Solid State Commun.* **1999**, *112*, 35.
(14) Terekhov, S. V.; Obraztsova, E. D.; Lobach, A. S.; Konov, V. I. *Appl. Phys. A* **2002**, *74*, 393.
(15) Zheng, B.; Li, Y.; Liu, J. *Appl. Phys. A* **2002**, *74*, 345.
(16) Bandow, S.; Rao, A. M.; Williams, K. A.; Thess, A.; Smalley, R. E.; Eklund, P. C. *J. Phys. Chem. B* **1997**, *101*, 8839.
(17) Jeong, T.; Kim, W.-Y.; Hahn, Y.-B. *Chem. Phys. Lett.* **2001**, *344*, 18.
(18) Chattopadhyay, D.; Galeska, I.; Papadimitrakopoulos, F. *Carbon* **2002**, *40*, 985.
(19) Itkis, M. E.; Perea, D. E.; Niyogi, S.; Rickard, S. M.; Hamon, M. A.; Hu, H.; Zhao, B.; Haddon, R. C. *Nano Lett.* **2003**, *3*, 309.
(20) Lobach, A. S.; Spitsina, N. G.; Terekhov, S. V.; Obraztsova, E. D. *Phys. Solid State* **2002**, *44*, 475.
(21) Qiu, J.; Li, Y.; Wang, Y.; Wang, T.; Zhao, Z.; Zhou, Y.; Li, F.; Cheng, H. *Carbon* **2003**, *41*, 2170.
(22) Okazaki, T.; Shinohara, H. *Chem. Phys. Lett.* **2003**, *376*, 606.
(23) Qian, W.; Liu, T.; Wei, F.; Yuan, H. *Carbon* **2003**, *41*, 1851.
(24) Kataura, H.; Kumazawa, Y.; Maniwa, Y.; Ohtsuka, Y.; Sen, R.; Suzuki, S.; Achiba, Y. *Carbon* **2000**, *38*, 1691.
(25) Dresselhaus, M. S.; Dresselhaus, G.; Jorio, A.; Souza Filho, A. G.; Saito, R. *Carbon* **2002**, *40*, 2043.
(26) Kataura, H.; Kumazawa, Y.; Maniwa, Y.; Umezu, I.; Suzuki, S.; Ohtsuka, Y.; Achiba, Y. *Synth. Met.* **1999**, *103*, 2555.
(27) Jost, O.; Gorbunov, A. A.; Pompe, W.; Pichler, T.; Friedlein, R.; Knupfer, M.; Reibold, M.; Bauer, H.-D.; Dunsch, L.; Golden, M. S.; Fink, J. *Appl. Phys. Lett.* **1999**, *75*, 2217.
(28) Landi, B. J.; Ruf, H. J.; Worman, J. J.; Raffaelle, R. P. *J. Phys. Chem. B* **2004**, *108*, 17089.
(29) Hu, H.; Zhao, B.; Itkis, M. E.; Haddon, R. C. *J. Phys. Chem. B* **2003**, *107*, 13838.
(30) Itkis, M. E.; Perea, D. E.; Niyogi, S.; Love, J.; Tang, J.; Yu, A.; Kang, C.; Jung, R.; Haddon, R. C. *J. Phys. Chem. B* **2004**, *108*, 12770.
(31) Sen, R.; Rickard, S. M.; Itkis, M. E.; Haddon, R. C. *Chem. Mater.* **2003**, *15*, 4273.
(32) Zhao, B.; Itkis, M. E.; Niyogi, S.; Hu, H.; Perea, D. E.; Haddon, R. C. *J. Nanosci. Nanotechnol.* **2004**, *4*, 995.

(33) Zhao, B.; Itkis, M. E.; Niyogi, S.; Hu, H.; Zhang, J.; Haddon, R. C. *J. Phys. Chem. B* **2004**, *108*, 8136.
(34) Ryabenko, A. G.; Dorofeeva, T. V.; Zvereva, G. I. *Carbon* **2004**, *42*, 1523.
(35) http://www.carbonsolution.com.
(36) Lebedkin, S.; Hennrich, F.; Skipa, T.; Kappes, M. M. *J. Phys. Chem. B* **2003**, *107*, 1949.
(37) Bachilo, S. M.; Benedetto, A. F.; Weisman, R. B. *J. Phys. Chem. A* **2001**, *105*, 9845.
(38) Dresselhaus, M. S.; Dresselhaus, G.; Eklund, P. C. *Science of Fullerenes and Carbon Nanotubes*; Academic Press: San Diego, CA, 1996.
(39) Endo, M.; Kim, Y. A.; Fukai, Y.; Hayashi, T.; Terrones, M.; Terrones, H.; Dresselhaus, M. S. *Appl. Phys. Lett.* **2001**, *79*, 1531.
(40) Rao, A. M.; Chen, J.; Richter, E.; Schlecht, U.; Eklund, P. C.; Haddon, R. C.; Venkateswaran, U. D.; Kwon, Y. K.; Tomanek, D. *Phys. Rev. Lett.* **2001**, *86*, 3895.
(41) Selection of "100%" as the naming convention for the purified SWNTs has been made for simplicity of constructing the sample set and interpretation of results.
(42) Lian, Y.; Maeda, Y.; Wakahara, T.; Akasaka, T.; Kazaoui, S.; Minami, N.; Choi, N.; Tokumoto, H. *J. Phys. Chem. B* **2003**, *107*, 12082.
(43) Lian, Y.; Maeda, Y.; Wakahara, T.; Akasaka, T.; Kazaoui, S.; Minami, N.; Shimizu, T.; Choi, N.; Tokumoto, H. *J. Phys. Chem. B* **2004**, *108*, 8848.
(44) Stockli, T.; Bonard, J.-M.; Chatelain, A.; Wang, Z. L.; Stadelmann, P. *Phys. Rev. B* **2001**, *64*, 115424.
(45) Shyu, F. L.; Lin, M. F. *Phys. Rev. B* **2000**, *62*, 8508.
(46) Shyu, F. L.; Lin, M. F. *Phys. Rev. B* **1999**, *60*, 14434.
(47) Lin, M. F. *Phys. Rev. B* **2000**, *62*, 13153.
(48) Lin, M. F.; Chuu, D. S.; Huang, C. S.; Lin, Y. K.; Shung, K. W.-K. *Phys. Rev. B* **1996**, *53*, 15493.
(49) Lin, M. F.; Shung, K. W.-K. *Phys. Rev. B* **1994**, *50*, 17744.
(50) Jiang, X. *Phys. Rev. B* **1996**, *54*, 13487.
(51) Lauret, J.-S.; Voisin, C.; Cassabois, G.; Delalande, C.; Roussignol, P.; Jost, O.; Capes, L. *Phys. Rev. Lett.* **2003**, *90*, 057404.
(52) Bose, S. M. *Phys. Lett. A* **2001**, *289*, 255.
(53) Pichler, T.; Knupfer, M.; Golden, M. S.; Fink, J.; Rinzler, A.; Smalley, R. E. *Phys. Rev. Lett.* **1998**, *80*, 4729.
(54) Jackson, J. D. Plane Electromagnetic Waves and Wave Propagation. In *Classical Electrodynamics*, 2nd ed.; John Wiley & Sons: New York, 1962; p 284.
(55) O'Connell, M. J.; Bachilo, S. M.; Huffman, C. B.; Moore, V. C.; Strano, M. S.; Haroz, E. H.; Rialon, K. L.; Boul, P. J.; Noon, W. H.; Kittrell, C.; Ma, J.; Hauge, R. H.; Weisman, R. B.; Smalley, R. E. *Science* **2002**, *297*, 593.
(56) Skoog, D. A.; Holler, F. J.; Nieman, T. A. *Principles of Instrumental Analysis*, 5th ed.; Harcourt Brace & Co.: Philadelphia, PA, 1998.
(57) Bachilo, S. M.; Strano, M. S.; Kittrell, C.; Hauge, R. H.; Smalley, R. E.; Weisman, R. B. *Science* **2002**, *298*, 2361.
(58) Hagen, A.; Hertel, T. *Nano Lett.* **2003**, *3*, 383.
(59) Weisman, R. B.; Bachilo, S. M. *Nano Lett.* **2003**, *3*, 1235.
(60) Hayashi, Y.; Yu, G.; Rahman, M. M.; Krishna, K. M.; Soga, T.; Jimbo, T.; Umeno, M. *J. Appl. Phys.* **2001**, *89*, 7924.
(61) Samsonidze, G. G.; Chou, S. G.; Santos, A. P.; Brar, V. W.; Dresselhaus, G.; Dresselhaus, M. S.; Selbst, A.; Swan, A. K.; Unlu, M. S.; Goldberg, B. B.; Chattopadhyay, D.; Kim, S. N.; Papadimitrakopoulos, F. *Appl. Phys. Lett.* **2004**, *85*, 1006.
(62) Bahr, J. L.; Mickelson, E. T.; Bronikowski, M. J.; Smalley, R. E.; Tour, J. M. *Chem. Commun.* **2001**, *2*, 193.
(63) Zhou, B.; Lin, Y.; Li, H.; Huang, W.; Connell, J. W.; Allard, L. F.; Sun, Y.-P. *J. Phys. Chem. B* **2003**, *107*, 13588.